Materials Today Communications 50 (2026) 114531

Contents lists available at ScienceDirect

Materials Today Communications

journal homepage: www.elsevier.com/locate/mtcomm

Microstructural studies on early-stage deformation in thin-walled LPBF-manufactured SS316L considering its printing orientation

Ved Prakash Dubey [a], Dominika Przygucka [b], Marzena Pawlik [c], Zbigniew L. Kowalewski [a], Paul Wood [c], Mateusz Kopec [a,c,*]

[a] Institute of Fundamental Technological Research, Polish Academy of Sciences, Pawinskiego 5B, Warsaw 02-106, Poland
[b] Faculty of Advanced Technologies and Chemistry, Military University of Technology, Warsaw 00-908, Poland
[c] Institute for Innovation in Sustainable Engineering, College of Science and Engineering, University of Derby, DE22 1GB, UK

ARTICLE INFO

Keywords:
Stainless steel
Microstructure
Additive manufacturing
Laser Powder Bed Fusion Melting (LPBF-M)

ABSTRACT

This study investigates the influence of build orientation on the microstructure and early-stage deformation behaviour of austenitic stainless steel 316 L (SS316L) produced via laser powder bed fusion (LPBF). Three LPBF specimen orientations: horizontal (XY), inclined at 45° (ZX), and vertical (Z) were compared to conventionally produced wrought SS316L. Mechanical testing was conducted under uniaxial tension to fracture and to a controlled axial strain of 1 % to capture the onset of plasticity. Electron backscatter diffraction (EBSD) was performed before and after deformation to quantify grain boundary character, misorientation distribution, and grain morphology evolution. The LPBF material exhibited notable differences in yield strength and strain hardening, with the Z-oriented specimens exhibiting the lowest mechanical performance due to insufficient interlayer bonding and elongated melt pool boundaries aligned with the build direction. In contrast, the XY and ZX orientations showed relatively higher strength and more uniform deformation behaviour. EBSD revealed that early-stage plastic deformation led to the intragranular misorientation accumulation but the degree of it varied significantly with orientation. Wrought SS316L displayed the highest overall mechanical properties and more homogeneous deformation due to its equiaxed, recrystallized microstructure.

1. Introduction

Additive manufacturing (AM) of metallic materials, particularly via laser powder bed fusion (LPBF), has attracted significant interest due to its ability to produce complex geometries with high precision and minimal material waste [1,2]. AM technologies has demonstrated the ability to produce a material that achieves superior mechanical properties even in the as-built state than the post-processed (like, heat-treated) by varying the process parameters [3,4]. Among stainless steels, austenitic stainless steel 316 L (SS316L) is widely studied owing to its excellent corrosion resistance, ductility, and biocompatibility, making it suitable for structural, biomedical, and marine applications [5]. Consequently, considerable research has focused on the fabrication of SS316L by LPBF, also referred to as selective laser melting (SLM). Advances in processing strategies and parameter optimization have enabled the production of components with relative densities exceeding 99 % [6]. Numerous studies have demonstrated that LPBF-fabricated SS316L exhibits a superior combination of strength and ductility at room temperature compared to conventionally cast or forged counterparts [7]. The suppression of large-scale defects has been directly linked to the enhanced ductility consistently reported in the literature [8,9]. These superior properties are primarily associated with distinctive microstructural features across multiple length scales, most notably, the formation of fine cellular/dendritic structures with characteristic sizes ranging from 0.4 nm to 1.5 μm. Microstructural analyses further attribute the improved performance to refined grains, a high fraction of low-angle grain boundaries, and the presence of a dense dislocation network [10–12].

Despite these advantages, LPBF-fabricated SS316L often exhibits mechanical anisotropy arising from its layer-by-layer build process, directional solidification, and melt pool morphology, resulting in epitaxial grain growth and the development of long columnar grains in the build direction. Owing to its single-phase nature, SS316L is particularly suitable for investigating and tailoring crystallographic textures through LPBF [13]. Previous studies have shown that build orientation significantly influences strength, ductility, and deformation

* Corresponding author at: Institute of Fundamental Technological Research, Polish Academy of Sciences, Pawinskiego 5B, Warsaw 02-106, Poland.
E-mail addresses: mkopec@ippt.pan.pl, M.Kopec@derby.ac.uk (M. Kopec).

https://doi.org/10.1016/j.mtcomm.2025.114531
Received 17 October 2025; Received in revised form 8 December 2025; Accepted 17 December 2025
Available online 17 December 2025

mechanisms, with vertically fabricated specimens (Z) often showing inferior performance compared to horizontally built ones (XY) due to weaker interlayer bonding and melt pool orientation effects [14–16]. More recent advances in texture control have enabled the fabrication of LPBF SS316L with tailored crystallographic orientations, ranging from random distributions to strong ⟨100⟩ or ⟨110⟩ textures aligned with the build direction. Sun et al. [17] reported a novel lamellar microstructure comprising alternating ⟨100⟩ and ⟨110⟩ grains, while Wang et al. [18] achieved single-crystalline-like bulk SS316L with a {110}⟨001⟩ Goss texture. These developments highlight the pronounced dependence of tensile behavior on crystallographic orientation, as confirmed by anisotropic responses along the $< 100 >$, $< 110 >$, and $< 111 >$ directions. Although, the most studies concentrated on tensile behaviour up to fracture, the microstructural processes governing the onset of plasticity during early-stage deformation remain still less explored.

The deformation of materials is inherently complex and represents a key challenge in engineering, as it involves fundamental nonequilibrium phenomena. These complexities become particularly evident once the applied load exceeds the linear elastic regime, at which point many metals begin to yield and plastic deformation initiates and further progress. It is now well established that plasticity does not proceed in a simple or uniform manner, but instead displays intricate and heterogeneous characteristics [19,20]. The regime immediately beyond the yield point, often referred to as early-stage plastic deformation or the microplasticity zone, is therefore not merely a continuation of elastic behavior but a distinct and critical phase. Within this regime, the fundamental mechanisms that govern plastic flow are first activated and progressively established, laying the foundation for the subsequent evolution of deformation [21,22].

Early-stage deformation involves microstructural processes such as slip system activation, local lattice rotations, and dislocation accumulation. From a materials design perspective, the ultimate objective is often to achieve enhanced combinations of strength and toughness. By understanding and controlling the mechanisms that govern the early stage deformation through strategies such as grain refinement, nano-precipitation, or transformation-induced plasticity, new alloys with tailored properties can be developed. Despite this importance, systematic studies that combine controlled-strain mechanical testing with detailed microstructural analysis remain limited for AM 316 L steels. In one of the recent study, Barkia et al. [23] performed in-situ SEM/EBSD tensile tests on direct energy deposition-manufactured SS316L along build orientation supported by TEM investigations at various strain levels. At small tensile strain (~1 %), SS316L showed minimal changes in dislocation structure, with heterogeneous cell walls formed by dense arrays interspersed with sparse regions. This limited evolution was linked to restricted mobility of pre-existing dislocations pinned at nodes and barriers, requiring higher stresses to activate glide. Moreover, to the best of authors' knowledge, there has been no research conducted on early stage deformation of LPBF SS316L for multiple orientations combining with EBSD analysis, nor directly compared such behaviour to that of wrought SS316L.

Therefore, this work aims to address this gap in our understanding by investigating the microstructural response of LPBF SS316L in three build orientations (XY, ZX, Z) under uniaxial tension to an imposed axial strain of 1 %. The results were compared against conventionally wrought SS316L to assess the role of AM-specific microstructure.

2. Materials and methods

2.1. Specimen fabrication

The SS316L specimens were fabricated using a Renishaw AM 250 laser powder bed fusion system with powder feedstock supplied by Renishaw. The system is equipped with a 200 W continuous-wave fiber laser (λ = 1070 nm, 70 μm spot size) and a build volume of 250 × 250 × 300 mm^3. Processing was conducted under a high-purity argon atmosphere, established by initial evacuation and backfilling, to minimize oxygen contamination during solidification. The LPBF parameters applied in this study are presented in Fig. 1a. A meander scanning strategy with a 67° rotation of the scanning direction after each layer was used for printing of the specimens.

Cylindrical bars with a nominal diameter of 13 mm and length of 70 mm were printed in three orientations relative to the build plate: vertical (Z), horizontal (XY), and 45° inclined (ZX), as shown in Fig. 1c. Following fabrication, stress relief heat treatment was performed at 470°C for 6 h while the parts remained attached to the build plate, in accordance with the standard practice. After cooling, the bars were separated from the plate by wire cutting and subsequently machined to obtain thin-walled tubular specimens with the geometry shown in Fig. 1b. Both inner and outer surfaces were precision machined under identical turning conditions to ensure uniformity.

2.2. Mechanical testing

Mechanical tests were carried out at room temperature (23°C) using an MTS 858 servo-hydraulic biaxial testing system with load and torque capacities of ±25 kN and ±100 Nm, respectively. Initial uniaxial tensile tests were performed to determine baseline material properties, including the 0.2 % offset yield strength (YS), ultimate tensile strength (UTS), and ductility. For subsequent experiments, thin-walled tubular specimens were instrumented with Vishay 120 Ω strain gauge affixed at the mid-gauge section to monitor axial strain. Tests were controlled up to 1 % axial strain, which was selected to capture the early-stage deformation regime. The thin-walled tubular specimen geometry ensures highly uniform axial stress and minimizes bending or constraint effects. This configuration is well-established for producing homogeneous strain fields during early deformation, and prior finite-element verification confirmed that strain gradients across the wall thickness were below 3 %. Therefore, the microstructural responses observed via EBSD are attributed to intrinsic material behaviour rather than specimen geometry.

2.3. Material characterisation using EBSD

Microstructural characterisation was conducted using electron backscatter diffraction (EBSD) on a FEI Quanta 3D FEG scanning electron microscope equipped with integrated EDS/EBSD detectors, operated at 20 kV. Sample preparation involved hot mounting followed by sequential polishing: planarization using a Struers MD-Largo disc with 2 μm diamond suspension, and final surface finishing on a Metrep® MD-Chem cloth with 0.04 μm colloidal silica solution. EBSD analyses were carried out both in the initial (non-deformed) condition and after tensile deformation up to 1 %.

3. Results and discussion

3.1. Mechanical parameters from tensile tests

The room temperature tensile properties and the corresponding engineering stress–strain curves of wrought SS316L and LPBF-fabricated SS316L specimens tested along three orientations under uniaxial tension until fracture were presented in Fig. 2a. It was observed, that wrought SS316L demonstrates higher strength and ductility compared to the AM counterparts. Specifically, the wrought material exhibits an UTS of 740 MPa and total elongation of 45 %, whereas the AM specimens show lower UTS values ranging between 660–713 MPa and reduced elongation to failure of only 22–40 % depending on the build orientation. Among the LPBF builds, the XY orientation has the highest UTS (713 MPa) and elongation (40 %), while the Z-oriented specimens consistently display the lowest UTS (660 MPa) and ductility (22 %). The ZX specimens, fabricated at a 45° inclination, show intermediate values

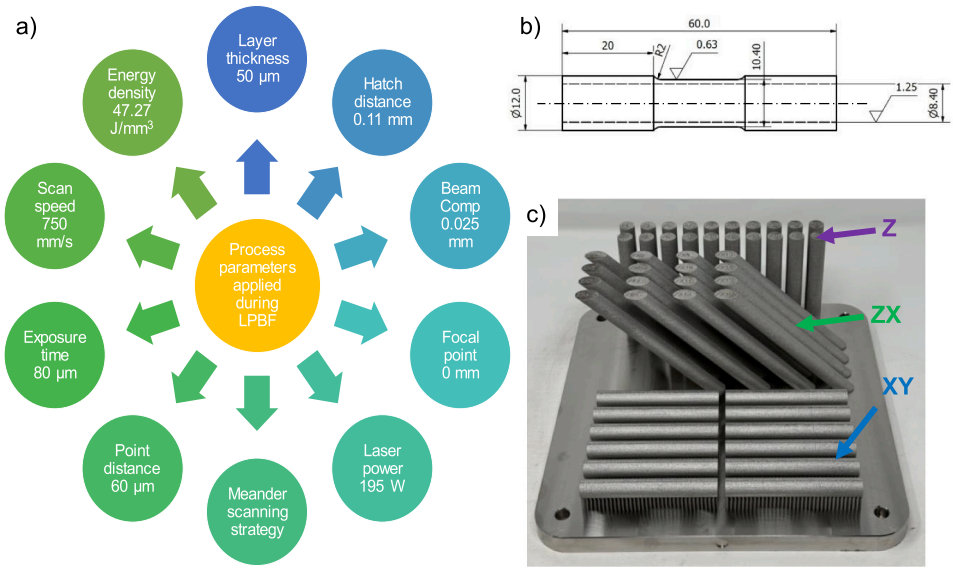

Fig. 1. Additive manufacturing process parameters (a); engineering drawing of the thin-walled tubular specimen (b); specimens printed in three orientations on the build plate (c).

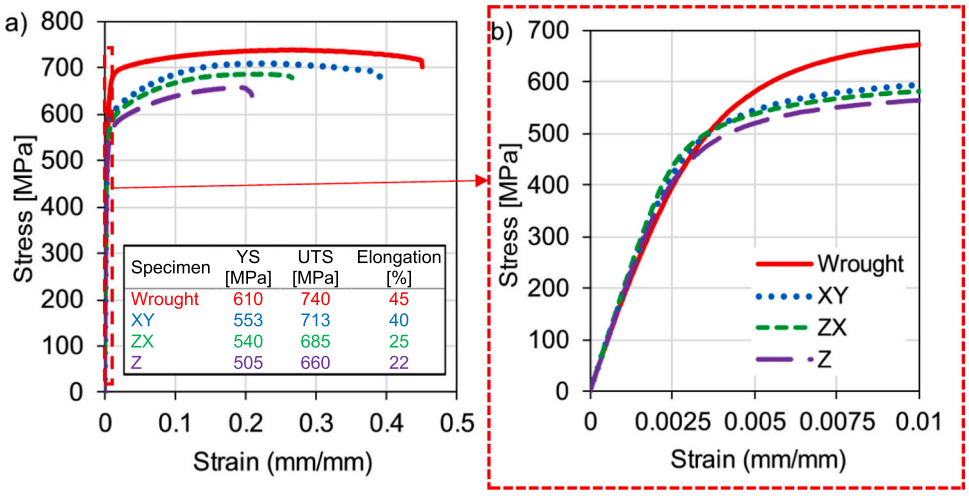

Fig. 2. Standard tensile characteristics of the wrought and additively manufactured SS316L (a); magnification of 1 % strain area (b).

(UTS = 685 MPa, elongation = 25 %). The reduced ductility in LPBF specimens, particularly in the Z direction, can be attributed to the presence of melt pool boundaries, layer-wise defects, grain boundary triple points and anisotropic grain morphologies aligned with the build direction. These microstructural heterogeneities act as preferential sites for void nucleation and crack propagation, thereby limiting tensile ductility. Although the LPBF-SS316L specimens investigated in this work exhibit lower tensile properties than the wrought counterpart, their mechanical performance remains significantly higher than that reported in the literature for SS316L fabricated by alternative routes, including wire arc additive manufacturing [24], electron beam powder bed fusion [25], laser-directed energy deposition [26], and conventional casting [27].

To gain further insight into the initial plastic response, Fig. 2b depicts the stress–strain behaviour magnified to the early deformation regime up to 1 % axial strain. The yield strength (YS) 0.2 % offset YS was determined for the wrought SS316L is determined to be 610 MPa, accompanied by a smooth and progressive strain-hardening response. In contrast, the LPBF specimens show distinct orientation-dependent differences in yield point values. The XY and ZX orientations exhibit higher YS values (553 MPa and 540 MPa, respectively) compared to the Z orientation (505 MPa), reflecting the influence of grain orientation and solidification texture induced by the layer-by-layer fabrication.

3.2. *Microstructural observations*

During the LPBF process, the strong thermal gradients that develop between the molten pool and the previously solidified layers promote directional solidification. The grain growth direction generally follows the maximum temperature gradient, i.e., normal to the melt pool boundary and approximately parallel to the build direction (Z-axis). Consequently, columnar grains in LPBF SS316L tend to elongate along the build direction, whereas equiaxed grains may form near the melt pool boundaries or in regions of reduced temperature gradient [28–30].

To evaluate texture evolution during plastic deformation, EBSD was performed on representative areas of wrought and AM SS316L specimens both before testing and after 1 % strain. The analysis provided quantitative insights into grain boundary character, misorientation distribution, and grain morphology. Fig. 3 presents the inverse pole figure (IPF) maps of wrought SS316L and AM-SS316L with respect to the

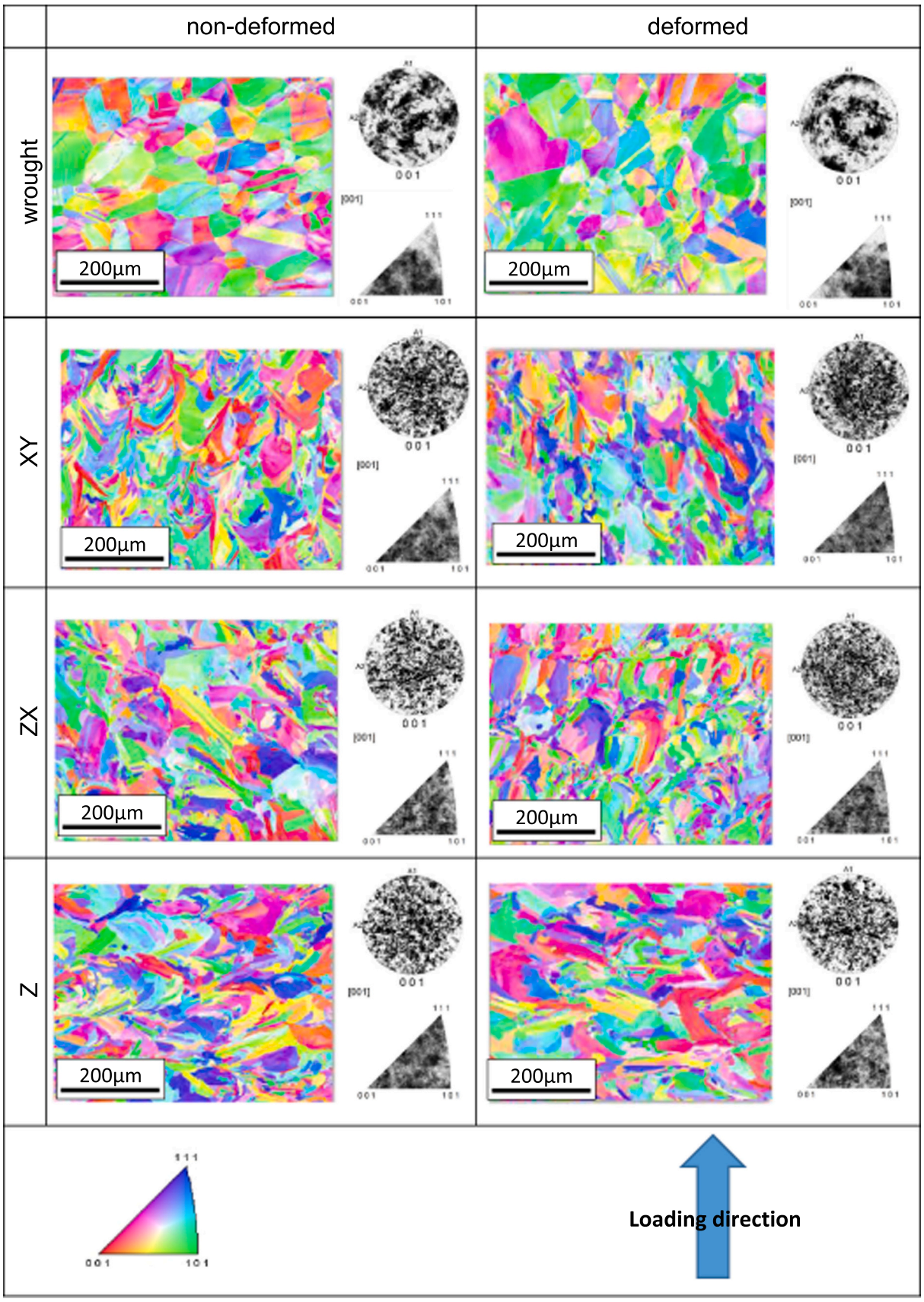

Fig. 3. IPF maps of SS316L specimens.

three build directions.

In the wrought SS316L, the non-deformed state shows equiaxed grains with relatively homogeneous morphology. Grain orientations show a near-random distribution with no specific texture. After 1 % tensile strain, the overall grain morphology remains unchanged, reflecting the material's stable grain structure at small values of strain, however, grain orientation dominantly shifted towards the $< 101 >$ crystallographic direction. In both conditions, however, twining was observed. In contrast, the LPBF SS316L specimens (XY, ZX, and Z orientations) exhibit highly elongated, irregular, and anisotropic grains in the non-deformed state, reflecting the directional solidification during laser powder bed fusion. Upon deformation to 1 %, these grains reveal pronounced intragranular orientation gradients and localized lattice rotations. This suggests a strong sensitivity of the AM microstructure to early plastic deformation, where pre-existing substructures (cellular solidification features and melt pool boundaries) serve as preferential sites for dislocation storage. The LPBF SS316L specimens exhibit random crystallographic texture in the non-deformed condition. However, after 1 % strain, no significant reorientation of the dominant texture components occurs at such small strain levels. Instead, deformation changed the orientation distribution, which is most pronounced in the XY orientation. This indicates that the restricted slip activity and anisotropic grain morphology in the XY direction promote localized lattice rotations from the earliest stages of plasticity [31]. This aligns directly with the observed mechanical anisotropy and reduced ductility in AM specimens.

Fig. 4 illustrates the grain distribution maps of the tested SS316L specimens. The EBSD grain distribution analysis reveals significant differences in misorientation angle characteristics between wrought and LPBF-manufactured SS316L specimens under both conditions. In wrought SS316L, deformation led to a notable increase in low-angle grain boundaries (LAGBs) (2°–5°) from 0.240 to 0.336 and in high-angle grain boundaries (HAGBs) (15°–180°) from 0.549 to 0.621. This indicates that during early plastic deformation the wrought microstructure accumulates dislocations and develops subgrain structures (increased LAGBs) in a relatively homogeneous manner without strong localization. The increase in HAGBs suggests some progressive lattice reorientation at grain boundaries, but not pronounced fragmentation. This behaviour is consistent with the EBSD maps that show small, uniform intragranular orientation gradients in the wrought material which attributed to the distributed geometrically necessary dislocation (GND) storage and multi-slip activity that delays localization. These observations correlate with the observed smooth strain hardening and higher ductility in the wrought specimens.

The AM specimens, however, displayed orientation-dependent responses. In the XY orientation, deformation resulted in an increase in LAGBs (0.240–0.276) and slight decrease in HAGBs (0.652–0.613). The increase in very low-angle boundaries indicates subgrain / GND formation during early plasticity, implying that the XY build accommodates strain by forming distributed dislocation structures rather than by abrupt grain rotation or fragmentation [32]. The negligible reduction in HAGB fraction suggests either subtle re-arrangement of misorientations within the measurement area or conversion of some high-angle boundaries into finer internal misorientation structure, possibly through intragranular subdivision.

The ZX orientation, representing a 45° inclination relative to the build platform, show the increase of HAGBs (0.674–0.716) combined with small decreases in LAGB fractions (0.217–0.200) suggests that early deformation in ZX promotes relatively localized lattice rotation or the conversion of existing subgrain boundaries into larger misorientations, which is resulted from the grain fragments/blocks that rotate away from their initial orientation. The Z orientation demonstrates a large decrease in LAGBs fraction (0.250–0.109) with a simultaneous increase in HAGBs (0.646–0.701) which indicates that, early deformation results in rapid enlargement of local misorientation either by coalescence of dense dislocation walls into larger-angle boundaries or by rigid body rotation of columnar grains leading to stronger neighbour misorientations [33]. The rapid LAGB-to-HAGB conversion can be attributed to the alignment of long columnar grains with the loading axis. This geometry promotes fast accumulation of dislocations against cellular walls, which subsequently coarsen or collapse into higher-angle boundaries. Additionally, the elongated grains experience small but rigid rotations under axial loading, further amplifying the misorientation transition. This emphasises that the Z orientation seems to favour localized lattice rotation or relative grain reorientation rather than the uniform accumulation of many small-angle GND walls. One should stress, that in the Z-oriented specimens, regions exhibiting the strongest intragranular misorientation gradients align with melt-pool boundaries parallel to the build direction. These interfaces are known for keeping lack-of-fusion defects in LPBF steels, and their spatial coincidence with lattice-rotation areas suggests that insufficient interlayer bonding contributes to the early localization behaviour. Additionally, the stability of the LPBF dislocation-cell network is strongly orientation-dependent. In XY and ZX orientations, the cell walls intersect the loading axis, facilitating distributed slip and stable GND accumulation. In contrast, in the Z-orientation many cell boundaries run parallel to the tensile axis, acting as strong dislocation barriers that rapidly saturate. Their subsequent rearrangement or collapse promotes abrupt lattice rotation and higher-angle boundary formation. The misorientation differences at 1 % strain provide early indicators of macroscopic tensile behaviour. The XY orientation, which develops numerous LAGBs and distributed GND structures, is expected to exhibit sustained strain hardening and enhanced ductility due to its capacity to accommodate slip homogeneously. Conversely, the Z-orientation shows rapid LAGB collapse and HAGB formation, signalling early strain localization and predicting lower work-hardening and reduced ductility—consistent with the tensile results in Section 3.1.

Although the present study focuses primarily on the identification of early-stage deformation mechanisms rather than on defect elimination strategies, the results directly reveal how key LPBF-specific microstructural features influence strain accommodation and anisotropic plastic response. The differences observed across the XY, ZX, and Z orientations arise not only from bulk texture and grain morphology but also from the hierarchical set of solidification-induced features—including melt-pool boundaries, interlayer interfaces, and cellular/dendritic dislocation networks. These features act as microstructural constraints that dictate the onset of slip, govern the accumulation and rearrangement of GNDs, and determine whether deformation proceeds through distributed lattice rotation or localized strain partitioning. Importantly, several of the microstructural zones that exhibit strong lattice curvature or elevated misorientation correspond spatially to melt-pool boundaries or build-layer interfaces, which are known from prior literature to contain lack-of-fusion porosity or incomplete metallurgical bonding. While quantifying porosity is outside the scope of this paper, the correlation between these characteristic AM interfaces and the early localization behaviour observed via EBSD highlights the relationship between LPBF process-derived defects and the mechanical anisotropy that emerges even at strains as low as 1 %. By revealing the strain-dependent response of these microstructural features at the very onset of plasticity, the present work provides mechanistic insight that is essential for guiding future optimization strategies. Specifically, these findings highlight the microstructural origins of anisotropy that must be addressed through improved scanning strategies, altered melt-pool geometry, or post-processing treatments aimed at homogenizing the cellular structure and enhancing interlayer bonding.

4. Concluding remarks

This study systematically studied the build orientation–microstructure–property relationships of stainless steel 316 L (SS316L) fabricated by laser powder bed fusion and highlight the role of early microstructural changes in anisotropic mechanical behaviour. The

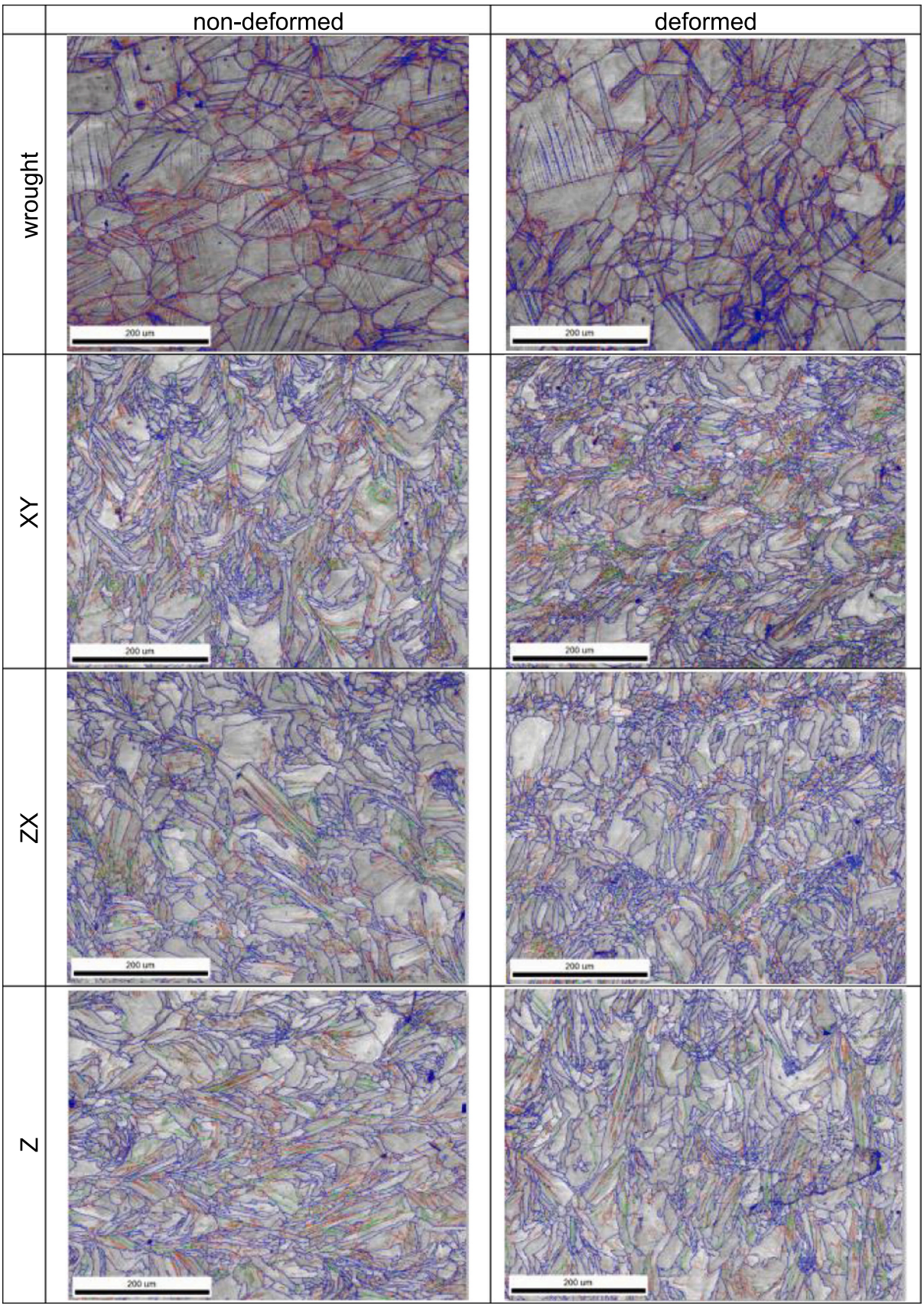

Fig. 4. Grain distribution maps of SS316L specimens.

following major conclusions are summarized as follows:

- LPBF SS316L exhibits significant orientation-dependent mechanical anisotropy, with Z-oriented specimens showing the lowest yield strength and ductility, while XY specimens the highest.
- EBSD analysis after 1 % axial deformation revealed that the early-stage plastic flow can be characterised by build orientation-dependent intragranular misorientation accumulation.
- Wrought SS316L outperformed LPBF material in strength and ductility due to its isotropic microstructure, showing homogeneous early-stage deformation.

CRediT authorship contribution statement

Ved Prakash Dubey: Writing – original draft, Formal analysis, Data curation, Conceptualization. **Dominika Przygucka:** Methodology, Investigation. **Zbigniew L. Kowalewski:** Writing – review & editing, Supervision, Project administration. **Paul Wood:** Writing – review & editing, Validation, Supervision, Resources, Methodology. **Marzena Pawlik:** Methodology, Investigation. **Mateusz Kopec:** Writing – original draft, Visualization, Validation, Project administration, Methodology, Investigation, Funding acquisition, Formal analysis, Data curation, Conceptualization.

Declaration of Competing Interest

The authors declare that they have no known competing financial interests or personal relationships that could have appeared to influence the work reported in this paper.

Acknowledgements

The authors would like to express their gratitude to Mr M. Wyszkowski and Mr. A. Chojnacki for their kind help during the experimental part of this work. This work was funded partly by the National Science Centre through the grants no. 2019/35/B/ST8/03151 and 2023/51/B/ST8/01751.

Data availability

Data will be made available on request.

References

[1] W.E. Frazier, Metal additive manufacturing: a review, J. Mater. Eng. Perform. 23 (6) (2014) 1917–1928, https://doi.org/10.1007/s11665-014-0958-z.
[2] P. Bajaj, A. Hariharan, A. Kini, P. Kürnsteiner, D. Raabe, E.A. Jägle, Steels in additive manufacturing: a review of their microstructure and properties, Mater. Sci. Eng. A 772 (2020) 138633, https://doi.org/10.1016/j.msea.2019.138633.
[3] I. Mierzejewska, T. Durejko, A. Antolak-Dudka, D. Zasada, M. Kopec, Unravelling enhanced mechanical properties of LENS-manufactured Ti-5553 alloy through interlayer dwell control without post-processing heat treatment, J. Alloy. Compd. 1039 (2025) 182893, https://doi.org/10.1016/j.jallcom.2025.182893.
[4] V.P. Dubey, S. Sharma, M. Kopec, Z. Kowalewski, Additive Manufacturing of Metal Matrix Composites. Fundamentals and Advances in Metal Matrix Composites, CRC Press, 2025, pp. 66–78.
[5] Y.N. Aditya, J. Vincic, M.J. Benoit, Effects of wire feeding direction on the deposition characteristics of 316L stainless steel in laser-directed energy deposition, Manuf. Lett. 43 (2025) 27–32, https://doi.org/10.1016/j.mfglet.2024.11.006.
[6] Z. Sun, X. Tan, S.B. Tor, W.Y. Yeong, Selective laser melting of stainless steel 316L with low porosity and high build rates, Mater. Des. 104 (2016) 197–204, https://doi.org/10.1016/j.matdes.2016.05.035.
[7] L. Liu, Q. Ding, Y. Zhong, J. Zou, J. Wu, Y.-L. Chiu, J. Li, Z. Zhang, Q. Yu, Z. Shen, Dislocation network in additive manufactured steel breaks strength–ductility trade-off, Mater. Today 21 (4) (2018) 354–361, https://doi.org/10.1016/j.mattod.2017.11.004.
[8] Z. Li, T. Voisin, J.T. McKeown, J. Ye, T. Braun, C. Kamath, W.E. King, Y.M. Wang, Tensile properties, strain rate sensitivity, and activation volume of additively manufactured 316L stainless steels, Int. J. Plast. 120 (2019) 395–410, https://doi.org/10.1016/j.ijplas.2019.05.009.
[9] E. Liverani, S. Toschi, L. Ceschini, A. Fortunato, Effect of selective laser melting (SLM) process parameters on microstructure and mechanical properties of 316L austenitic stainless steel, J. Mater. Process. Technol. 249 (2017) 255–263, https://doi.org/10.1016/j.jmatprotec.2017.05.042.
[10] M.S. Pham, B. Dovgyy, P.A. Hooper, Twinning induced plasticity in austenitic stainless steel 316L made by additive manufacturing, Mater. Sci. Eng. A 704 (2017) 102–111, https://doi.org/10.1016/j.msea.2017.07.082.
[11] Y.J. Yin, J.Q. Sun, J. Guo, X.F. Kan, D.C. Yang, Mechanism of high yield strength and yield ratio of 316 L stainless steel by additive manufacturing, Mater. Sci. Eng. A 744 (2019) 773–777, https://doi.org/10.1016/j.msea.2018.12.092.
[12] A.J. Birnbaum, J.C. Steuben, E.J. Barrick, A.P. Iliopoulos, J.G. Michopoulos, Intrinsic strain aging, Σ3 boundaries, and origins of cellular substructure in additively manufactured 316L, Addit. Manuf. 29 (2019) 100784, https://doi.org/10.1016/j.addma.2019.100784.
[13] L. Cui, S. Jiang, J. Xu, R.L. Peng, R.T. Mousavian, J. Moverare, Revealing relationships between microstructure and hardening nature of additively manufactured 316L stainless steel, Mater. Des. 198 (2021) 109385, https://doi.org/10.1016/j.matdes.2020.109385.
[14] M. Kopec, V.P. Dubey, M. Pawlik, P. Wood, Z.L. Kowalewski, Experimental identification of yield surface for additively manufactured stainless steel 316L under tension–compression-torsion conditions considering its printing orientation, Manuf. Lett. 41 (2024) 28–32, https://doi.org/10.1016/j.mfglet.2024.07.003.
[15] H.H. Alsalla, C. Smith, L. Hao, Effect of build orientation on the surface quality, microstructure and mechanical properties of selective laser melting 316l stainless steel, RPJ 24 (1) (2018) 9–17, https://doi.org/10.1108/RPJ-04-2016-0068.
[16] P. Wood, T. Libura, Z.L. Kowalewski, G. Williams, A. Serjouei, Influences of horizontal and vertical build orientations and post-fabrication processes on the fatigue behavior of stainless steel 316L produced by selective laser melting, Materials 12 (24) (2019) 4203, https://doi.org/10.3390/ma12244203.
[17] S.-H. Sun, T. Ishimoto, K. Hagihara, Y. Tsutsumi, T. Hanawa, T. Nakano, Excellent mechanical and corrosion properties of austenitic stainless steel with a unique crystallographic lamellar microstructure via selective laser melting, Scr. Mater. 159 (2019) 89–93, https://doi.org/10.1016/j.scriptamat.2018.09.017.
[18] X. Wang, J.A. Muñiz-Lerma, M. Attarian Shandiz, O. Sanchez-Mata, M. Brochu, Crystallographic-orientation-dependent tensile behaviours of stainless steel 316L fabricated by laser powder bed fusion, Mater. Sci. Eng. A 766 (2019) 138395, https://doi.org/10.1016/j.msea.2019.138395.
[19] S. Papanikolaou, Y. Cui, N. Ghoniem, Avalanches and plastic flow in crystal plasticity: an overview, Model. Simul. Mater. Sci. Eng. 26 (1) (2017) 013001, https://doi.org/10.1088/1361-651X/aa97ad.
[20] L.B. Zuev, V.I. Danilov, S.Y. Zavodchikov, On the initial stage of plastic deformation of metal alloys, J. Mater. Eng. Perform. 9 (2) (2000) 170–173, https://doi.org/10.1361/105994900770346123.
[21] H. Yang, W. Zhang, X. Zhuang, Z. Zhao, Experimental and modeling investigation on anisotropic plastic flow of metal plates under nonproportional loading conditions, Int. J. Solids Struct. 309 (2025) 113174, https://doi.org/10.1016/j.ijsolstr.2024.113174.
[22] M. Zhou, Q. Wang, S. Chen, S. Takagi, K. Ichiyanagi, S. Nozawa, R. Fukaya, J. Li, L. Xu, Y. Yu, Q. Wu, J. Hu, First in situ observation of partial dislocation-mediated plastic flow in shocked single-crystal aluminum, Ultra Sci. 5 (2025) 0111, https://doi.org/10.34133/ultrafastscience.0111.
[23] B. Barkia, M. Vallet, A. Tanguy, T. Auger, E. Héripré, New insights into microstructure evolution and deformation mechanisms in additively manufactured 316L stainless steel, Mater. Sci. Eng. A 934 (2025) 148327, https://doi.org/10.1016/j.msea.2025.148327.
[24] R. Sasikumar, A.R. Kannan, S.M. Kumar, R. Pramod, N.P. Kumar, N.S. Shanmugam, Y. Palguna, S. Sivankalai, Wire arc additive manufacturing of functionally graded material with SS 316L and IN625: microstructural and mechanical perspectives, CIRP J. Manuf. Sci. Technol. 38 (2022) 230–242, https://doi.org/10.1016/j.cirpj.2022.05.005.
[25] C. Wang, X. Tan, E. Liu, S.B. Tor, Process parameter optimization and mechanical properties for additively manufactured stainless steel 316L parts by selective electron beam melting, Mater. Des. 147 (2018) 157–166, https://doi.org/10.1016/j.matdes.2018.03.035.
[26] A. Aversa, A. Saboori, E. Librera, M. de Chirico, S. Biamino, M. Lombardi, P. Fino, The role of directed energy deposition atmosphere mode on the microstructure and mechanical properties of 316L samples, Addit. Manuf. 34 (2020) 101274, https://doi.org/10.1016/j.addma.2020.101274.
[27] D. Benjamin, C.W. Kirkpatrick, ASM Metals Handbook, Properties and Selection: Stainless Steels, Tool Materials and Special-Purpose Metals, Met. Handbook, 9th Edn, 3, American Society of Metals, 1980.
[28] Jincheng Wang, Rui Zhu, Yujing Liu, Laichang Zhang, Understanding melt pool characteristics in laser powder bed fusion: an overview of single- and multi-track melt pools for process optimization, Adv. Powder Mater. 2 (4) (2023) 100137, https://doi.org/10.1016/j.apmate.2023.100137.
[29] D. Wang, S. Li, G. Deng, et al., A melt pool temperature model in laser powder bed fabricated CM247LC Ni superalloy to rationalize crack formation and microstructural inhomogeneities, Met. Mater. Trans. A 52 (2021) 5221–5234, https://doi.org/10.1007/s11661-021-06457-5.
[30] Xianglong Wang, Jose Alberto Muñiz-Lerma, Mohammad Attarian Shandiz, Oscar Sanchez-Mata, Mathieu Brochu, Crystallographic-orientation-dependent tensile behaviours of stainless steel 316L fabricated by laser powder bed fusion, Mater. Sci. Eng. A 766 (2019) 138395, https://doi.org/10.1016/j.msea.2019.138395.
[31] Hongqiao Qu, Jing Li, Fucai Zhang, Jiaming Bai, Anisotropic cellular structure and texture microstructure of 316L stainless steel fabricated by selective laser melting

via rotation scanning strategy, Mater. Des. 215 (2022) 110454, https://doi.org/10.1016/j.matdes.2022.110454.

[32] C. Bean, F. Wang, M.A. Charpagne, P. Villechaise, V. Valle, S.R. Agnew, D. S. Gianola, T.M. Pollock, J.C. Stinville, Heterogeneous slip localization in an additively manufactured 316L stainless steel, Int. J. Plast. 159 (2022) 103436, https://doi.org/10.1016/j.ijplas.2022.103436.

[33] Yuanjian Hong, Chengshuang Zhou, Yuanyuan Zheng, Lin Zhang, Jinyang Zheng, The cellular boundary with high density of dislocations governed the strengthening mechanism in selective laser melted 316L stainless steel, Mater. Sci. Eng. A 799 (2021) 140279, https://doi.org/10.1016/j.msea.2020.140279.